



Two characteristic cellulose nanocrystals (CNCs) obtained from oxalic acid and sulfuric acid processing

Wei Jia · Yun Liu 

Received: 18 January 2019 / Accepted: 14 August 2019 / Published online: 19 August 2019
© Springer Nature B.V. 2019

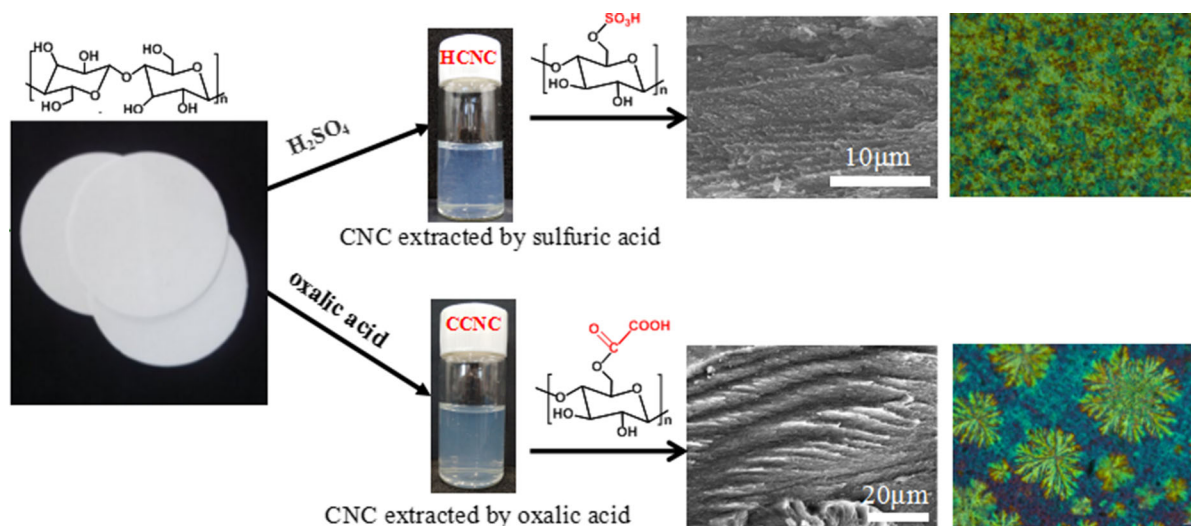
Abstract We systematically compare the different properties of cellulose nanocrystals (CNCs) obtained by oxalic acid and sulfuric acid hydrolysis methods. The variant characteristics of two kinds of CNCs were confirmed by XRD, DLS, Zeta, TGA, and SEM techniques. When CNCs were mixed with PEG, and the chiral nematic tissue of CNCs was retained in the solid film to observe the liquid crystal phase by evaporation-induced self-assembly. The brilliant

snowflake-like pattern of CNC film was observed through oxalic acid instead of sulfuric acid. More importantly, carboxylated CNCs prepared by oxalic acid was easily formed a liquid crystal phase by adding cationic solutions into 1.27% CNC solution. The extra properties of CNCs obtained by oxalate dihydrate contribute to its potential application prospects in optical devices and chiral separation.

Electronic supplementary material The online version of this article (<https://doi.org/10.1007/s10570-019-02690-9>) contains supplementary material, which is available to authorized users.

W. Jia · Y. Liu (✉)
College of Life Science and Technology, Beijing
University of Chemical Technology, No.15 Beisanhuan
East Road, Chaoyang District, Beijing 100029, China
e-mail: liyun@mail.buct.edu.cn;
liyunprivate@sina.com

Graphic abstract



Keywords Oxalate dihydrate · Sulfuric acid · Cellulose nanocrystals (CNCs) · Evaporation-induced self-assembly (EISA) · CNC liquid crystal phase

Introduction

Cellulose nanocrystals (CNCs) have recently attracted much considerable attention due to their unique properties including large surface area, low density, high mechanical properties, renewability and biodegradability (Zhang and Liu 2018). To date, CNCs has been widely used as optical materials (Yao et al. 2017), conductive materials (Liu et al. 2017), tissue engineering substrates (Dong et al. 2013), nematic liquid crystal materials (Shopsowitz et al. 2010) and bulk chemicals. Inorganic acid hydrolysis is the prominent method for CNC production, including sulfuric acid (Reid et al. 2017; Shopsowitz et al. 2010), hydrochloric acid (Kontturi et al. 2016) and phosphotungstic acid (Lu et al. 2016). However, these inorganic acids always cause defects to some content, such as requiring large amount of acid (about 9 kg H_2SO_4 per kg CNCs), low yield of CNCs (20–30%), and long reaction time (30 h) (Hamad and Hu 2010), as well as equipment corrosion and releasing waste water. To meet the above-mentioned challenge, organic acids assisted by ultrasonic or mixing with inorganic acids have been emerged to yield CNCs

(Filson and Dawson-Andoh 2009; Tang et al. 2013). Using maleic acid as an example to hydrolyze biomass not only obtain CNC material, but also can functionalize CNC surface (Chen et al. 2016). In the latest years, although TEMPO oxidation has been conducted to prepare CNCs since it can break the amorphous area of cellulose, it has a long way to go in real application because of its high cost, toxic and corrosive nature (Zhou et al. 2018).

Regardless of the hydrolytic method for obtaining CNCs, its optical properties play a critical role in optical devices and chiral separation. Shopsowitz et al. (2011, 2014) reported that CNCs extracted by sulfuric acid hydrolysis could form liquid crystal phase, and they investigated the unique self-assembly conditions of nanocellulose suspension—chiral nematic liquid crystal phase. Giese et al. (2015) envisioned that the chiral nematic tissues of CNCs was retained in solid films through evaporation-induced self-assembly (EISA). These films usually displayed brilliant rainbow colors because of the one-dimensional photon properties of chiral nematic liquid crystal phases. It was found that tactoids were one of the most primitive components of liquid crystals. Wang observed the arrangement of cellulose nanocrystals within individual tactoid for the first time, and followed the structural evolution of the liquid crystalline phase from tactoids to iridescent-layered films (Wang et al. 2016). Although many studies on the optical properties of CNCs obtained by sulfuric acid have been

available in the literature, the optical properties of CNC by organic acids mostly remains unknown, and the influence of inorganic and organic acids hydrolysis strategies on the optical properties of CNCs has not been reported so far.

Herein, CNCs from filter paper was first obtained by oxalic acid under different conditions according to the method reported by Li et al. (2017) Oxalic acid was chosen because it is produced from biomass and easily recovered at low temperatures through crystallization processes to achieve sustainable and economical manufacturing. Oxalic acid has three roles in this present work, it acts not only as acid catalyst but also as reaction solvent as well as reactant. It can esterify with the C6 group of cellulose to obtain carboxylated CNCs. The procedure of oxalic acid hydrolysis toward CNCs was simple with nontoxicity and high yield, which was considering as green and sustainable proposal to prepare CNCs. Then, the structural characteristics of CNCs obtained by oxalic acid and sulfuric acid are elucidated in detail through XRD, DLS, Zeta, TGA, and SEM techniques. Finally, CNCs was mixed with PEG and the chiral nematic tissue of CNCs was retained in solid film by EISA. The optical properties observed with a polarizing microscope of the CNCs prepared by oxalic and sulfuric acids are significantly different.

Materials and methods

Materials

Qualitative filter paper (XinXing brand, China) was used as the raw material, its contents of cellulose, hemicellulose, ash and water were calculated to 89.42%, 5.11%, 2.09% and 1.88% respectively, according to standard NREL Laboratory Analytical Procedures (Sluiter et al. 2012). Tetrahydrofuran (THF, AR) and sulfate (AR) were purchased from Beijing Chemical Factory (Beijing, China). Oxalate dihydrate (AR) was bought from Aladdin Co. (Shanghai, China). Phosphotungstate hydrate (AR) was gained from Beijing Balinway Technology Co., Ltd (Beijing, China). Polyethylene glycol 20,000 (AR) was from Biotopped Co. (Beijing, China). Other reagents of sodium nitrate (AR), cobalt nitrate (AR), aluminum nitrate nonahydrate (AR), ferric nitrate (AR) were purchased from Xilong Chemical Co., Ltd

(Guangdong, China). Zinc nitrate (AR) and copper nitrate (AR) were brought from Tianjin Beilian chemicals development Co. Ltd (Tianjin, China). All the chemicals used in this work have not been further purified prior to usage.

CNC preparation by oxalic acid and sulfuric acid hydrolysis

The filter paper (FP) was cut into 3×3 mm (about 3 g) pieces for CNC preparation. For oxalic acid (OA) hydrolysis, the major parameters affecting CNC yield were optimized at 110 °C and 300 r/min, including oxalic acid dosages (5.75, 8.75, 11.75 g oxalate dihydrate/g filter paper) and reaction times (15 min, 30 min, 60 min, 120 min). Specifically, amount of OA was weighed and put into a 250 mL three-necked flask, which was heated in oil bath to 110 °C. Under this temperature, OA was melt into liquid phase. Then, 3 g FP was added into the flask and hydrolysis reaction was started at the stirring rate of 300 r/min. After designed reaction interval, the hydrolysis reaction was stopped. Then 30 mL hot deionized water was put into the flask, withdrawing the solution into the beaker and filtering immediately. The residue solid was washed with 60 mL THF at 55 °C until the filtrate was colorless and its pH was neutral. After THF vaporization, CNC hydrolysis by OA was obtained and denoted as COX according to different OA dosage and reaction time. Amount of COX was suspended into 300 mL deionic water to reach the final concentration of 0.5%. pH of the suspension solution was adjusting to 9–10 with 0.1 M NaOH. After ultrasonic treatment over JY98-IIIDN ultrasonic instrument (Ningbo Scientz Biotechnology Co., Ltd, China) with the power of 720 W for 60 min, CNC solution by oxalic acid was finally achieved and denoted as CCNC because of carboxylation at C6 group in the cellulose. The CCNC solution was stored in the refrigerator at 4 °C for the following experiments.

For sulfuric acid hydrolysis, 64% (w/w) of sulfuric acid was used as acid catalyst. For CNC preparation, 8.75 mL H_2SO_4 /g FP was conducted to hydrolyze filter paper at 45 °C for 45 min and then filtered under vacuum. The filtrate was mixed with distilled water ($\times 10$) thoroughly for 20 min and then centrifuged at 26 °C. It repeated three times. The suspension was obtained and dialyzed against distilled water in dialysis bag with a molecular weight cutoff of 8000–14,000

(Biotopped, Beijing, China) for 5 days until a pH neutral solution was obtained. After ultrasonic treatment for 60 min, CNC solution by sulfuric acid was finally achieved and denoted as HCNC.

Preparation of CNC composite film

CNC composite films were prepared according to the method reported by Yao et al. (2017). In detailed, 3% CNC solution of two as-obtained samples were mixed with 10% PEG solution. The mixture solution was homogenized for 24 h at speed rate of 700 r/min, followed by ultrasonic dispersion for 3 min. And then the suspension was poured into a plastic petri dish and dried at room temperature to obtain the composite films. As controls, two kinds of CNC films without PEG were prepared only using CCNC and HCNC as feed stocks, respectively.

Fabrication of CNC liquid crystal phase

The CNC liquid crystal phase was prepared according to the procedure in detail by Zander et al. (2014). In short, 500 μL of CNCs (1.27 wt%) were added to 2 mL centrifuge tube, and then 500 μL of metal ionic solutions, including NaNO_3 , $\text{Zn}(\text{NO}_3)_2$, $\text{Cu}(\text{NO}_3)_2$, $\text{Co}(\text{NO}_3)_2$, $\text{Fe}(\text{NO}_3)_3$, $\text{Al}(\text{NO}_3)_3$, were added to the centrifugal tube drop by drop at room temperature. The concentration of ionic solutions was ranging from 0.05 to 1.0 M. Leaving the centrifuge tube overnight and discarding the supernatant, the CNC liquid crystal phase was observed under the polarized light microscope (POM).

The structural properties of CNC samples

UV-Vis spectroscopy observation

The transmittance of CCNC and HCNC samples were respectively scanned on an UV756CRT ultraviolet spectrophotometer (Shanghai Youke Instrument Co. Ltd, China) in the wavelengths ranging from 200 to 900 nm (Li et al. 2016).

Oxalic acidification degree of CCNC analyzed by HPLC

Oxalic acid degree of CCNC was confirmed by high performance liquid chromatograph (HPLC)

to determine oxalic acid content according to H_2SO_4 hydrolysis. The H_2SO_4 hydrolysis procedures and HPLC conditions were detailed in our previous report (Schutyser et al. 2018; Zhou et al. 2016).

FT-IR analysis

The FT-IR spectra were recorded over FT-IR spectroscopy (VERTEX 80v, Bruker, USA) from 400 to 4000 cm^{-1} at a resolution of 1 cm^{-1} to explore the absorption peaks variances of feedstocks and samples in this work (Gan et al. 2017).

Nuclear magnetic resonance analysis

The structure of CCNCs was measured on 300 MHz nuclear magnetic resonance (NMR) spectrometer (AV-300, Bruker) (Abraham et al. 2017).

DLS and Zeta analysis

Zeta potential of CNC suspension was measured by electrophoresis laser scattering (Nano ZS, Malvern, UK). The diameter size of CNC suspension was determined by dynamic light scattering (DLS). The concentration of CNC suspension was fixed at 0.5 wt%. The detailed procedure was described in the literature (Reid et al. 2017).

Transmission electron microscopy (TEM) images

The morphology of CNCs was observed on the HT7700 Hitachi TEM (Hitachi, Japan) and its particle size distributions were analyzed by an image analysis system (Image J). The concentration of CNCs was fixed as 0.01 wt%. The detailed procedure was described in the literature (Kang et al. 2018).

X-ray diffraction (XRD) analysis

The crystalline degree of CNCs was obtained using an X-ray diffractometer (Bruker, Germany) with Ni-filtered $\text{Cu K}\alpha$ radiation at 40 kV and 40 mA (Gan et al. 2017). XRD diffraction data were collected from $2\theta = 5^\circ - 45^\circ$, and each sample was tested for 10 min. The crystalline index (CrI) of cellulose was

calculated by the peak height method (Park et al. 2010) according to Eq. (1).

$$Crl(\%) = \frac{I_{200} - I_{AM}}{I_{200}} \quad (1)$$

where I_{200} represents peak value at $2\theta = 22.6^\circ$ and I_{AM} is the peak value at $2\theta = 18.3^\circ$.

The characterization of CNC composite films

Weight changes of the films during drying

To study the changes of films' mass during evaporation, the solution mass was weighed per 12 h as a function of time.

UV-Vis spectroscopy of composite films

The transmission of composite films was determined on UV756CRT ultraviolet spectrophotometer (Shanghai Youke Instrument Co., Ltd, China) in the wavelength range of 400 to 1100 nm according to the procedures reported in the literature (Yao et al. 2017).

POM images of composite films

The optical characteristics of CNC composite films was determined on Axioskop 40 Pol polarizing microscope (Zeiss, Germany). The film samples were placed on the loading platform and POM images were observed under the red filter of polarizing microscope.

SEM images of composite films

The cross section morphology of CNC composite films was characterized on S-4700 Hitachi SEM (Japan). Prior to image, the CNC film samples were glued on the carrier platform and sprayed with gold. The detailed procedure was described in the literature (Fernandes et al. 2017).

TGA analysis of composite films

The thermal stability of CNC composite films was characterized with a DTG-60A thermal gravimetric analyzer (TGA, Shimadzu, Japan). Approx. 10 mg of sample were cut into tiny particles, and then heated from 40 to 800 °C at the heating rate of 10 °C min⁻¹ in nitrogen atmosphere. The flow rate of nitrogen was set at 50 mL min⁻¹.

Results and discussion

Effect of oxalic acid and H₂SO₄ hydrolysis on the basic structural properties of CNCs

The effect of oxalic acid dosage and reaction time on CNC yield and grafted oxalic acid content was investigated and the results are shown in Table 1. It can be seen that CCNC yield increases with the increasing of oxalic acid dosage when reaction time remains stable. However, when oxalic acid is fixed, CCNC yield decreases with increasing of reaction

Table 1 CCNC yield and grafted oxalic acid content under different conditions

Oxalic acid dosage (%)	Reaction time (min)	CCNC denoted name	CCNC yield (%)	oxalic acidification content (mmol/g)
5.75	15	CCNC-O5.75T15	86.78	0.32
5.75	30	CCNC-O5.75T30	80.56	0.40
5.75	60	CCNC-O5.75T60	74.16	0.43
5.75	120	CCNC-O5.75T120	72.67	0.37
8.75	15	CCNC-O8.75T15	93.77	0.29
8.75	30	CCNC-O8.75T30	72.05	0.44
8.75	60	CCNC-O8.75T60	71.19	0.54
8.75	120	CCNC-O8.75T120	69.82	0.32
11.75	15	CCNC-O11.75T15	93.74	0.33
11.75	30	CCNC-O11.75T30	88.86	0.40
11.75	60	CCNC-O11.75T60	76.74	0.38
11.75	120	CCNC-O11.75T120	72.83	0.24

time. The highest CCNC yield (93.77%) was obtained under the conditions of 8.75% oxalic acid and reaction time 15 min. CNC yield extracted by oxalic acid is higher than by H_2SO_4 hydrolysis reported in the literature (Li et al. 2016; Mishra et al. 2011; Yarbrough et al. 2017). In addition, esterification of cellulose at C2, C3 and C6 with oxalic acid is a rapid process within 15 min, and the content of oxalic acid grafted on CCNC is measured to be 0.3–0.54 mmol/g. Although high oxalic acid concentration can reduce cellulose cross-linking of CNC, however, it will enhance esterification degree between oxalic acid and cellulose to achieve the maximal carboxylation (de Melo et al. 2009; Li et al. 2017). When oxalic acid dosage is 8.75 g OA/g FP and the reaction time is 60 min, the highest value of 0.54 mmol/g the content of oxalic acid grafted on CCNC is obtained in this study. Therefore, oxalic acid plays three roles as acid catalyst, reaction substrate and solution medium in CCNC preparation from biomass.

The transmittance of CCNC suspension was examined by UV–Vis observation. As seen from Fig. 1a, the transmittance of 0.5 wt% CCNC suspension reaches 95% (Fig. 1a), indicating that CCNC solution is uniform, dispersal and the particles do not aggregate (Li et al. 2016). Interestingly, effect of oxalic acid dosage on the transmittance of CCNC shows limited (Fig. S1a, b). Similarly, the transmittance of 0.5 wt% HCNC suspension reaches 97.6% (Fig. S3a). In order to verify esterification reaction between oxalic acid and cellulose, FT-IR and NMR spectrum were employed to examine carbonyl group generation.

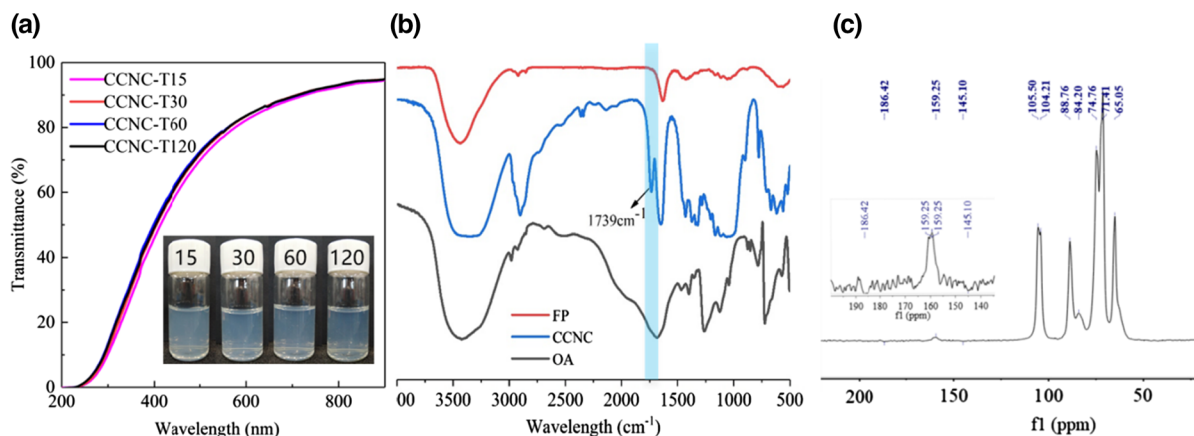


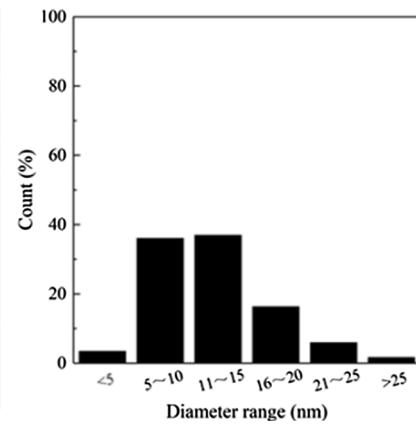
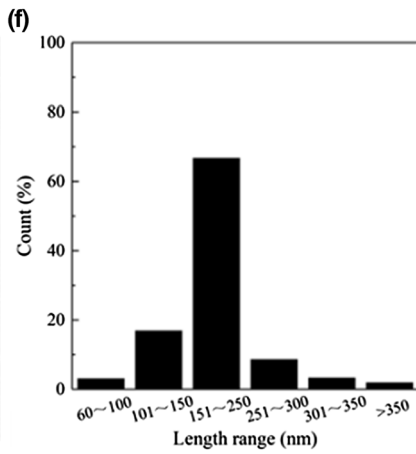
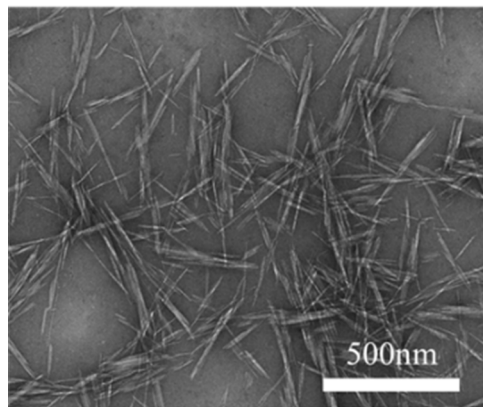
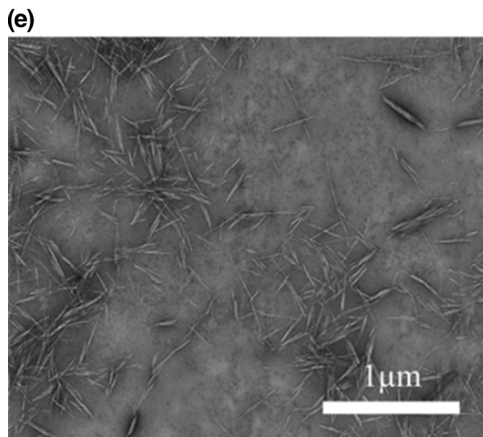
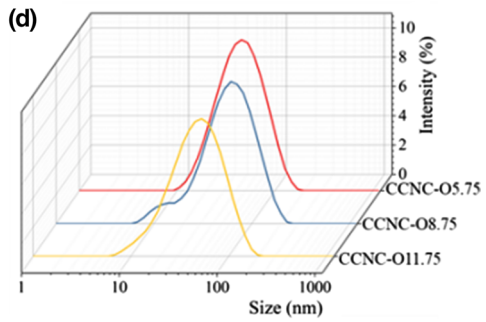
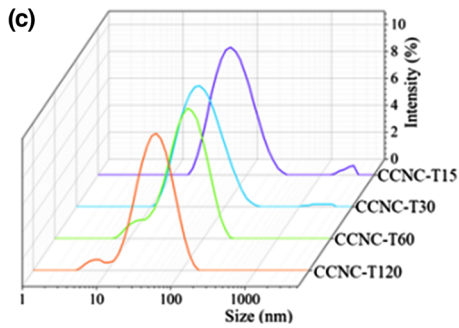
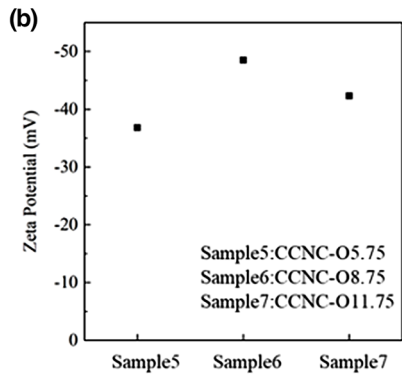
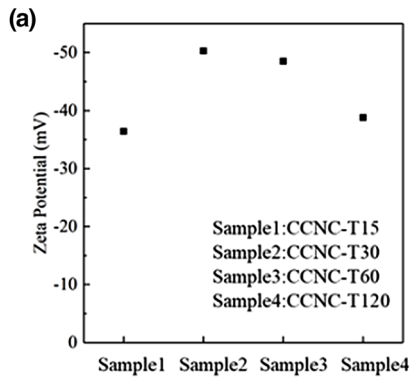
Fig. 1 **a** UV–Vis transmittance of 0.5 wt% CCNC suspensions. **b** FT-IR of filter paper (FP), oxalic acid (OA) and CCNC. **c** ^{13}C NMR spectrum of CCNC-O8.75T60. CCNC preparation conditions: reaction time 60, oxalic acid dosage 8.75 g OA/g FP

Fig. 2 **a** and **b** Zeta potential plot of seven kinds of CCNC under the conditions of 60 min and 8.75 g OA/g FP. **c** and **d** DLS measurement of seven kinds of CCNC under the conditions of 60 min and 8.75 g OA/g FP. **e** TEM images of the CCNC-O8.75T60. **f** Particle size distribution of the CCNC-O8.75T60

The FT-IR spectra of CCNC sample in Fig. 1b show a new peak at 1739 cm^{-1} , corresponding to the vibration of $\text{C}=\text{O}$ (Teramura et al. 2016). It confirms the esterification reaction between oxalic acid and cellulose, and the ester bond is probably located at C6 group in cellulose (Li et al. 2017). Through NMR analysis (Fig. 1c), an obvious peak appears at 160 ppm, corresponding to the vibration of $\text{C}=\text{O}$ ester (Abraham et al. 2017; Li et al. 2017), it also demonstrates the successful esterification of cellulose and oxalic acid. Thus, the carboxylated CNCs can be one-step obtained through hydrolysis and esterification by oxalic acid.

Further structural properties, including Zeta potential, particle size, morphology and Crl value, of CCNCs were also investigated, and effects of reaction time and oxalic acid dosage on the structural properties of CCNC were shown in Figs. 2 and 3.

Figures 2a and b show that the charges of CCNC samples are between -35 and -50 analyzed by Zeta potential test, which provide a solid guarantee that CCNC suspension is highly stable and transparent without precipitation observed in Fig. 1a. It was reported that high carboxyl content would result in a large negative surface charge, indicating the electrostatic stability of CCNC suspension (Bian et al. 2017).



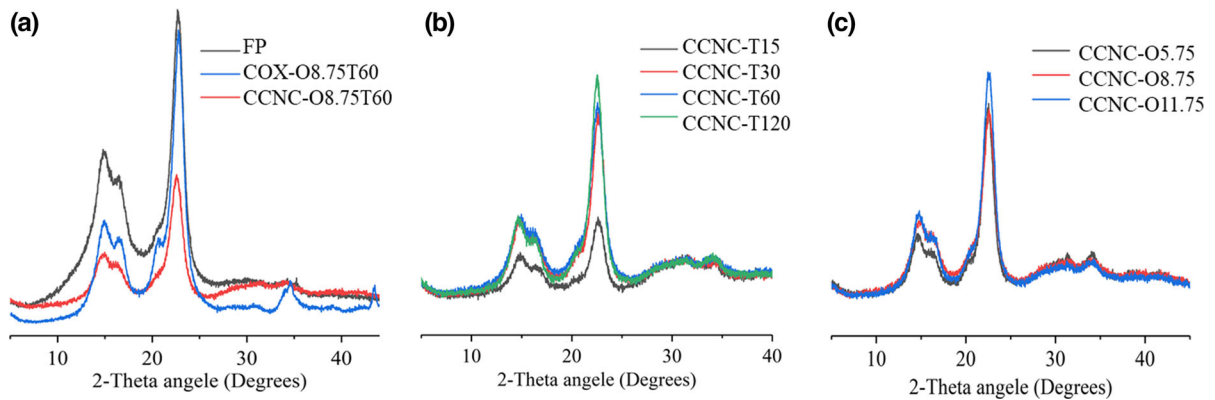


Fig. 3 **a** XRD patterns of the filter paper, COX-O8.75T60 and CCNC-O8.75T60. **b** Effect of reaction time on XRD patterns of CCNC. **c** Effect of oxalic acid on XRD patterns of CCNC

From DLS profiles in Fig. 2c and d, average particle sizes of CCNCs are within 10–100 nm, and parameters of oxalic acid dosage and reaction time show no significant effect on CCNC average particle sizes. The morphology of CCNCs was observed by TEM, the length and particle size distribution were statistically summarized in Figs. 2f and S2. From TEM images, it is shown that CCNC displays rod-shaped morphology with the length of 151–250 nm and particle size distribution of 5–20 nm. It is worthily noticed that oxalic acid dosage and reaction time show limited influence on CCNC length and particle size distributions (Fig. S2).

The crystal degree of CCNC was calculated by peak height method (Gan et al. 2017). As seen from the XRD profiles in Fig. 3, the CrI of filter paper, COX-O8.75T60 and CCNC-O8.75T60 is 79.62%, 88.73%, and 86.64%, respectively. The reasonable explanation is the fact that oxalic acid will interrupt the amorphous area of cellulose leading to the CrI enhancement. Through ultrasonic treatment for CCNC preparation, the structure of CCNC was damaged and its CrI was slightly decreased. As shown in Fig. 3b, with the elongation of reaction time, the CrI value of CCNC slightly increases, which is consistent with that reported in the literature (Chen et al. 2016). However, oxalic acid dosage (from 5.75 to 11.75 g/gPF) shows little effect on the CrI value in this study (Fig. 3c).

As control, the structural properties of HCNC prepared by H_2SO_4 were also characterized in this work and the results are depicted in Fig. S3. Like CCNC, the transmittance of HCNC is 97.6%, and no aggregation is not formed through UV–Vis

spectroscopy observation (Fig. S3a). As seen in Fig. S3b, the average particle size of HCNC is approx. 63.66 nm with uniform distribution. The Zeta potential of HCNC is -59.7 (Fig. S3c), slightly higher than that of CCNC (-50). As description before, high Zeta potential of CNC makes CNC suspension high electrostatic stability, it is very important for the formation of chiral phase. In addition, the CrI value of HCNC is calculated to be 91.72% by peak height method from XRD spectrum (Fig. S3d).

From these data, a conclusion has been drawn that CCNC and HCNC have the similar basic structural properties, such as UV–Vis transmittance, average particle size, Zeta potential and CrI value.

Effect of oxalic acid and H_2SO_4 hydrolysis on CNC composite film properties

Evaporation-induced self-assembly (EISA) method was employed to prepare CNC composite films, and the influence of oxalic acid and H_2SO_4 hydrolysis on CNC composite films properties was examined. The photos of CNC composite films observed in Fig. 4a and b, the appearance of both HCNC and CCNC composite films shows no difference under the black background. It is worthily noticed that the mass of CNC composite films decreases linearly as the function of time in the process of film formation through EISA, $m = 4.324 - 0.0531t$, $R^2 = 0.9992$, (m is liquid mass, g; t stands for the drying time, h) (Fig. 4c, d). However, UV–Vis observation shows that the transmittance of HCNC composite film (87%) is a little more transparent than that of CCNC composite film (84%).

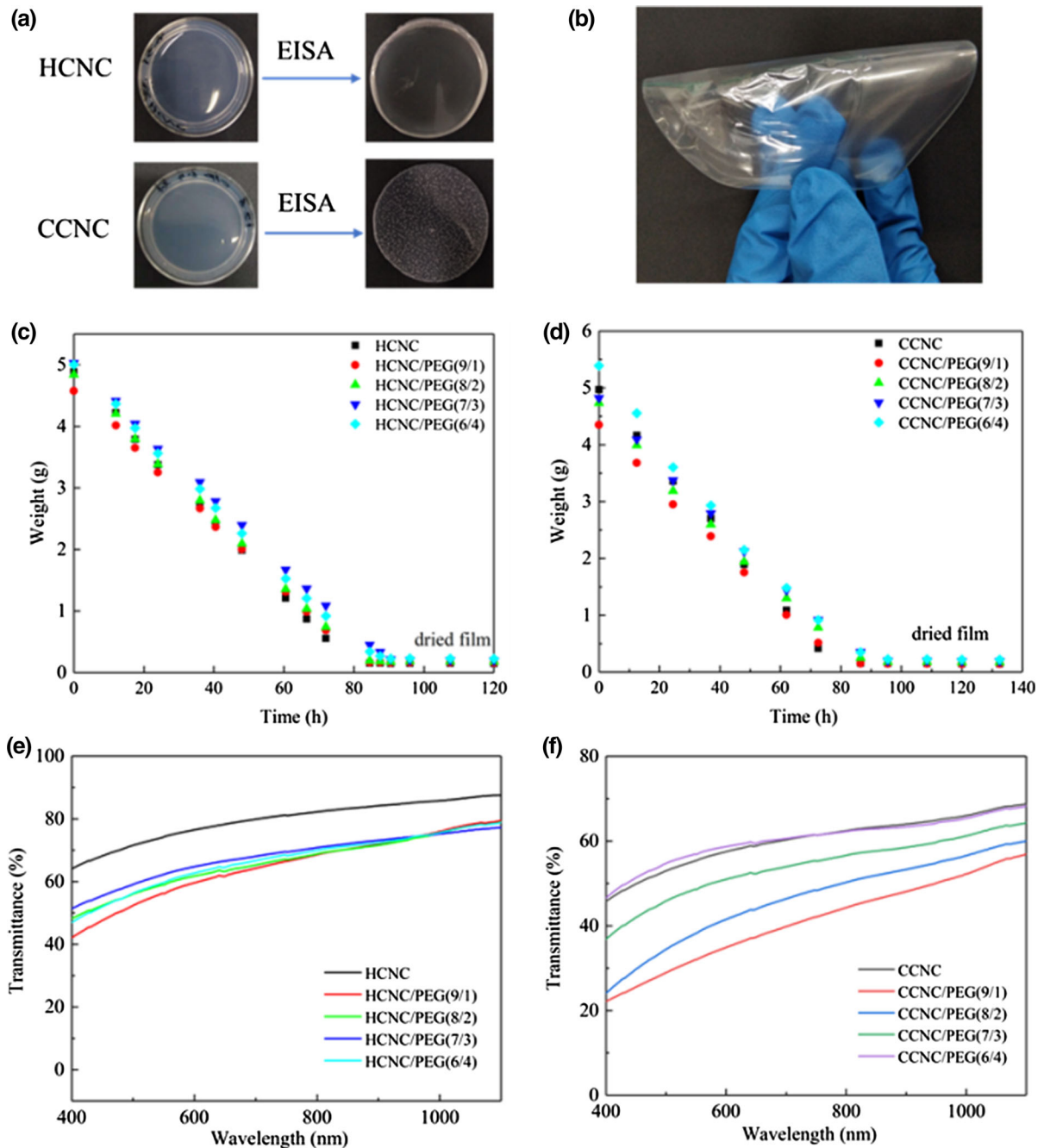


Fig. 4 **a** and **b** The photos of CNC composite films. **c** and **d** Mass variance of CNC composite film as the function of evaporation time. **e** and **f** UV-Vis observation of CNC composite films

The transmittance of CNC composite film increases when adding amount of PEG (Fig. 4e, f).

Furthermore, CCNC composite films show absolutely different optical property from HCNC composite film although both kinds of CNC composite films

present brilliant colors (Fig. 5). As seen in Fig. 5a, with increasing PEG content in composite film, POM images color of HCNC composite films change from green to yellow, and show texture fingerprint features. It is speculated that the chiral nematic structure of

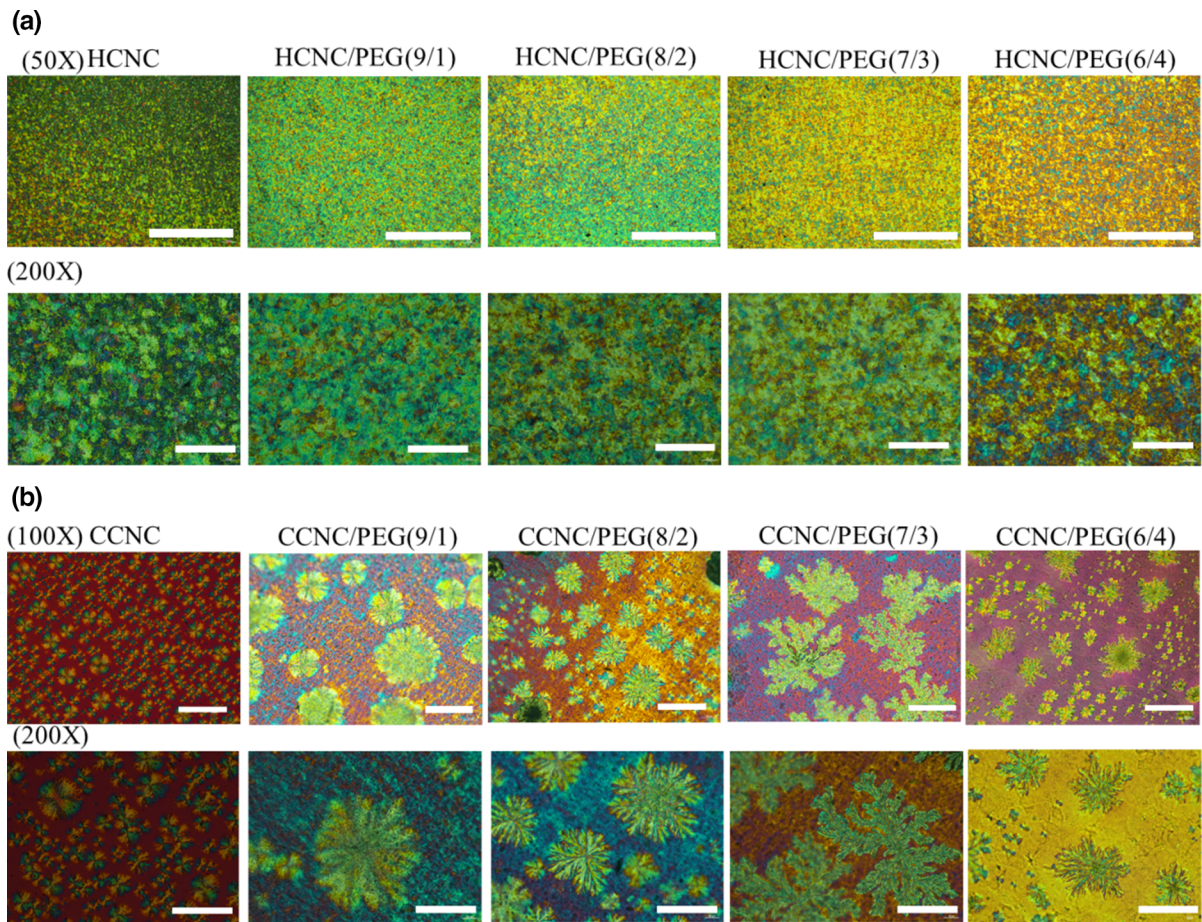


Fig. 5 **a** POM images of HCNC composite films at $50\times$ (*scale bar*, 1 nm) and $200\times$ (*scale bar*, 200 μm) magnification. **b** POM images of CCNC composite films at $100\times$ (*scale bar*, 500 μm) and $200\times$ (*scale bar*, 200 μm) magnification

CNCs is generated through CNCs self-assembly, which is confirmed by SEM in Fig. 6d. On the contrary, POM images of CCNC composite films display a unique colorful snow-flake patterns (Fig. 5b). It is probably attributed to the surface grafting reaction between carboxyl groups in CCNC and hydroxyl groups in PEG. This grafting reaction is a reversible reaction. When adding a drop of water onto the half surface of CCNC composite films, the colorful snow-flake patterns in the wetting part of the films become completely transparent and colorless (Shopsowitz et al. 2010). The birefringence of the CCNC/PEG composite films is drastically reduced even disappears when water is absorbed (Fig. S4b). While the films are dried again, the birefringence phenomena is visual. These changes are reversible and the films fully regain their iridescence and

birefringence upon drying (Shopsowitz et al. 2010). For HCNC composite films, the chiral nematic structure of remains still clearly visible when adding a drop of water on the surface of HCNC films (Fig. S4a). The significant difference in optical properties between CCNC and HCNC composite films may be attributed to refractive index matching between the isotropic liquid in the films. The ability to switch between iridescent and colourless films will find a potential promising applications in smart materials.

In order to explain POM image difference in optical properties between CCNC and HCNC composite films, their cross sections were observed by SEM to explore the CNCs self-assembly, and the results are depicted in Fig. 6. In comparison HCNC film without PEG (Fig. 6a) with HCNC/PEG(7/3) composite film

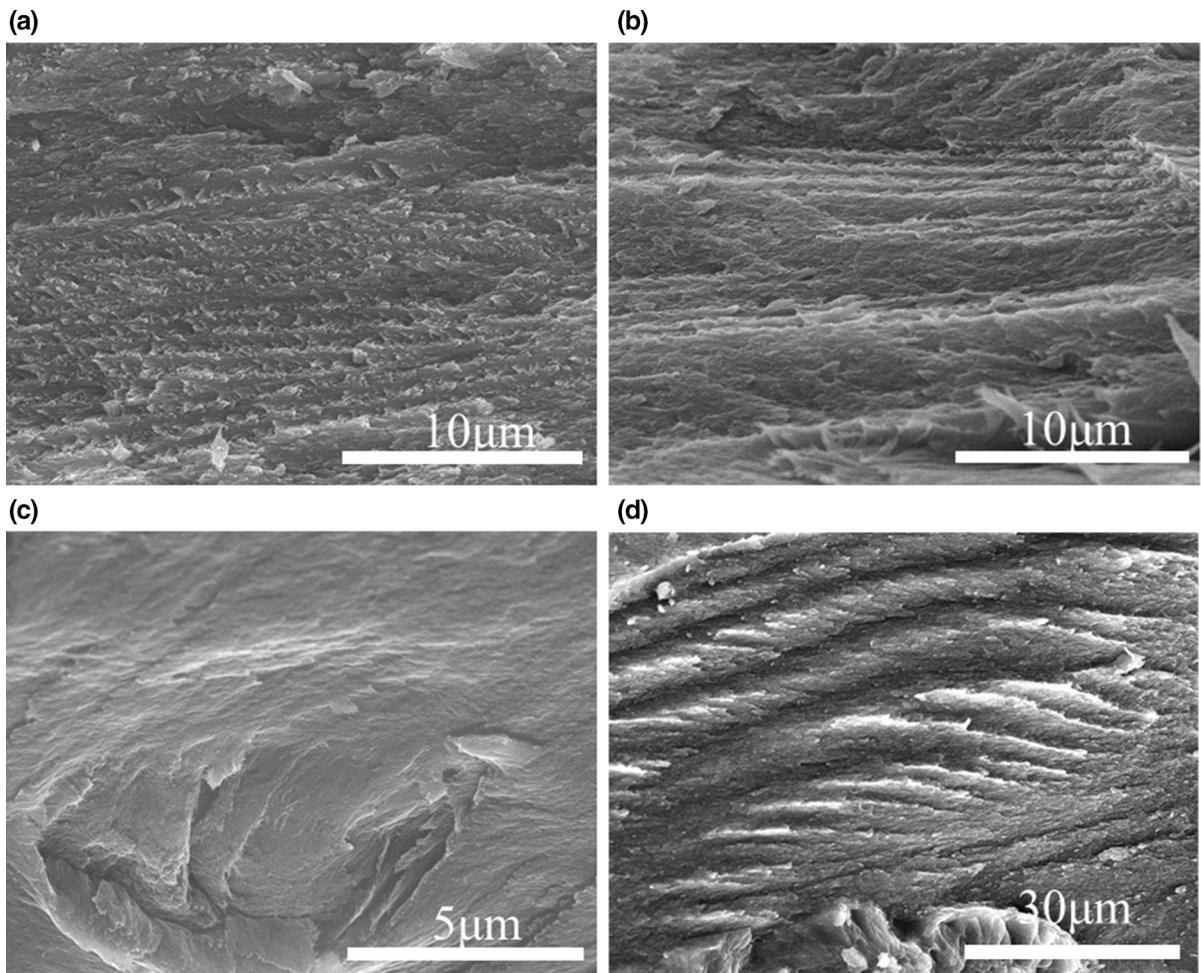


Fig. 6 **a** SEM image of cross section of HCNC film. **b** SEM image of cross section of HCNC/PEG(7/3) film. **c** SEM image of cross section of CCNC film. **d** SEM image of cross section of CCNC/PEG(7/3) film

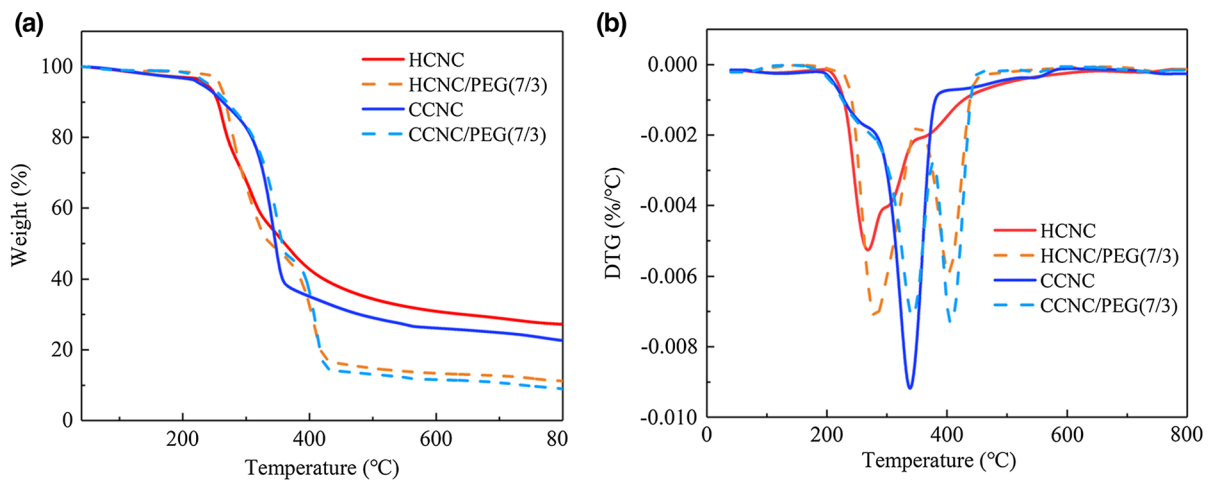
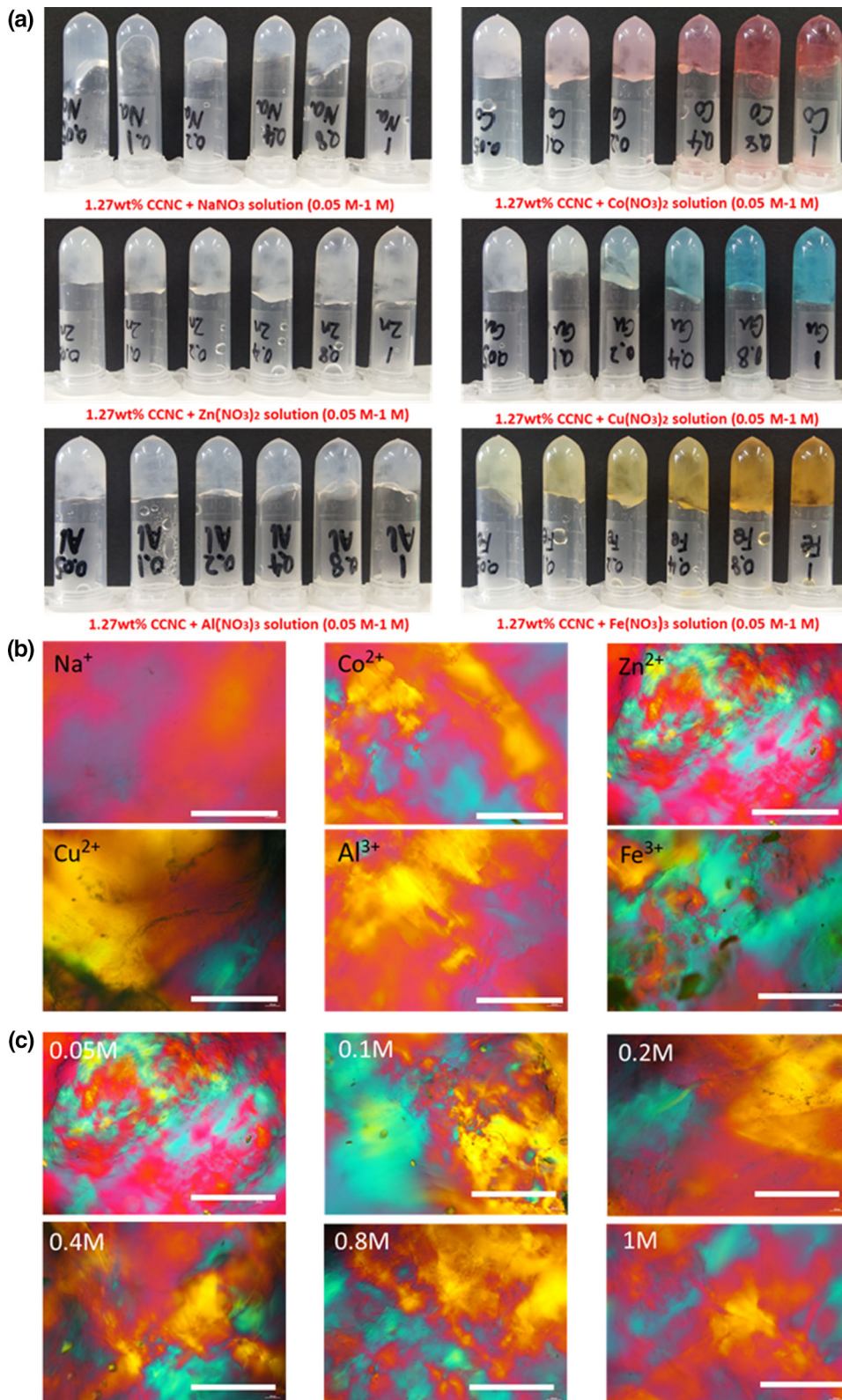


Fig. 7 Thermal stability of CNC/PEG composite films. **a** TGA curve of CNC films; **b** DTG curve of CNC films



◀ **Fig. 8** **a** Photos of CCNC (1.27 wt%) hydrogels reduced by adding cations solution with the concentrations ranging from 0.05 to 1.0 M. **b** POM images of CCNC hydrogels (*scale bar*, 1 μm). **c** Effect of Zn^{2+} concentration on POM images of CCNC hydrogels (*scale bar*, 1 μm)

(Fig. 6b), the multilayer and uniform structure with chirality sequence are observed, resulting in the characteristics of photon. However, for CCNC film without PEG, the cross section shows spherical multilayer spiral structure (Fig. 6c). For CCNC/PEG(7/3) composite film, it clearly shows uniform and multilayer structure. Therefore, the uniform spherical spiral structure of CCNC is probably contributed to the unique optical property observed by POM in Fig. 5b.

Thermal stability plays a crucial role for optical materials because oxidation degradation will always spoil the color of these materials (Yao et al. 2017). Effect of PEG addition on the thermal stability of CNC composite films was investigated through TGA/DGA analysis, and the results are summarized in Fig. 7. Two major points can be withdrawn from comparative analyses of Fig. 7: (1) the weight loss of HCNC and CCNC films without PEG addition is divided into 3 stages, dehydrate ($\geq 250\text{ }^\circ\text{C}$), decomposition ($250\text{--}380\text{ }^\circ\text{C}$) and slow carbonization ($380\text{--}600\text{ }^\circ\text{C}$); while the weight loss of CNC/PEG composite films is divided into 4 stages, dehydrate ($\geq 250\text{ }^\circ\text{C}$), decomposition ($250\text{--}350\text{ }^\circ\text{C}$), decomposition ($350\text{--}410\text{ }^\circ\text{C}$) and slow carbonization ($410\text{--}600\text{ }^\circ\text{C}$). (2) Adding PEG will enhance the decomposition temperature of CNC composite films by approx. $20\text{--}50\text{ }^\circ\text{C}$ (Fig. 7b). This improvement of thermal stability can be attributed to the formation of PEG protective layer on the surface of CNC, which is similar to the thermal decomposition of cellulose nanofiber grafted PEG reported in the literature (Tang et al. 2015). Compared with HCNC composite films, CCNC composite films have higher thermal stability and higher heat resistance, which was also confirmed in the literature (Chen et al. 2016).

The liquid crystal phase of CCNC hydrogel reduced by adding cation ions

CCNC suspension prepared by oxalic acid hydrolysis can easily form hydrogels with variant kinds of metal cation ions, including univalent cation (Na^+), bivalent

cations (Co^{2+} , Zn^{2+} , Cu^{2+}) and trivalent cations (Al^{3+} , Fe^{3+}). The mechanism for cation-promoted liquid crystal phase formation of CCNC in hydrogels was detailed in our previous work (Zhang and Liu 2018). CCNC gels were initiated by adding 500 μL cation solutions at concentrations ranging from 0.05 to 1.0 M to 1.27 wt% CCNC suspension with equivalent volume. CCNC suspension was gelatinized with all kinds of metal cation ions. The stability of the gel was confirmed by using inverted vials and the photos are shown in Fig. 8a. As expected, the binding force between monovalent ion (e.g. Na^+) and carboxylic acid is the weakest, then bivalent cations (Co^{2+} , Zn^{2+} , Cu^{2+}) and trivalent cations (Al^{3+} , Fe^{3+}) show the strongest binding force. It is probably a charge repulsion and shielding effect on the surface of the fibril bonded by strong cationic-carboxylate (Dong et al. 2013). The CCNC-cation ions formation gel does not have fluidity even with shaking and maintains the shape in vial. However, when the metal ions are drop by drop added to the vial filled with HCNC suspension, the flocculent phenomenon and some gels at the bottom of vial are observed. After being stationary overnight, the vial is upside down and it is found the gel is unstable and fluxed when shaken (Fig. S5a).

The optical properties of CCNC gels were characterized by POM technique, their images are shown in Fig. 8b. Apart from monovalent Na^+ , other metal bi- and trivalent ions gelation with CCNC present brilliant polarizing features (Fig. 8b). Using Zn^{2+} as a model (Fig. 8c), it is interesting to reveal that the brilliant polarizing feature of gel is independence of metal cation ions concentration (from 0.05 to 1.0 M). This brilliant polarizing feature may be caused by CCNC orderly arrangement in gel (Dong et al. 1996). Although HCNC can form unstable liquid crystal phase with metal cation ions (Fig. S5a), the brilliant polarizing feature of gel is not obvious (Fig. S5b) (Lagerwall et al. 2014). Therefore, brilliant polarizing feature of CCNC gel will be used as crystal template, sensor and chiral separation devices.

Conclusions

In this study, carboxylated CNCs from biomass is prepared by one-step hydrolysis and esterification through oxalic acid method. The whole procedure is simple, environmental friendly and cost-effective with

high CNC yield of 71–93%. The optical properties of CCNC extracted by oxalic acid show significant difference from HCNC extracted by traditional sulfuric acid method. On one hand, when CCNC is mixed with PEG, composite films of liquid crystal phase are obtained by EISA and CCNC composite films present brilliant color snowflake patterns under POM observation. On the other hand, CCNC hydrogels of liquid crystal phase are successfully formed by adding cation ions with different valence states into 1.27% CCNC solution. The CCNC hydrogels show brilliant polarizing feature due to CCNC rearrangement in an orderly manner. Therefore, the findings in our work provide a strategy for the extraction of functional CNCs from biomass, and these CNCs have potential application prospects in optical devices and chiral separation.

Acknowledgments This study was financially funded by the National Natural Science Foundation of China (NSFC, 21476016; 21776009).

Authors' contributions YL supervised the project, conceived the experiments and wrote the manuscript. WJ performed the experiments and co-wrote the manuscript.

Compliance with ethical standards

Conflict of interest The authors declare that they have no conflict of interest.

References

- Abraham E, Weber DE, Sharon S, Lapidot S, Shoseyov O (2017) Multifunctional cellulosic scaffolds from modified cellulose nanocrystals. *ACS Appl Mater Interfaces* 9:2010–2015. <https://doi.org/10.1021/acsami.6b13528>
- Bian H, Chen L, Dai H, Zhu JY (2017) Integrated production of lignin containing cellulose nanocrystals (LCNC) and nanofibrils (LCNF) using an easily recyclable di-carboxylic acid. *Carbohydr Polym* 167:167–176. <https://doi.org/10.1016/j.carbpol.2017.03.050>
- Chen L, Zhu JY, Baez C, Kitin P, Elder T (2016) Highly thermal-stable and functional cellulose nanocrystals and nanofibrils produced using fully recyclable organic acids. *Green Chem* 18:3835–3843. <https://doi.org/10.1039/c6gc00687f>
- de Melo JCP, Filho ECDS, Santana SAA, Airoidi C (2009) Maleic anhydride incorporated onto cellulose and thermodynamics of cation-exchange process at the solid/liquid interface. *Colloids Surf A Physicochem Eng Asp* 346:138–145. <https://doi.org/10.1016/j.colsurfa.2009.06.006>
- Dong XM, Kimura T, Revol JF, Gray GD (1996) Effects of ionic strength on the isotropic-chiral nematic phase transition of suspensions of cellulose crystallites. *Langmuir* 12:2076–2082
- Dong H, Snyder JF, Williams KS, Andzelm JW (2013) Cation-induced hydrogels of cellulose nanofibrils with tunable moduli. *Biomacromol* 14:3338–3345. <https://doi.org/10.1021/bm400993f>
- Fernandes SN et al (2017) Mind the microgap in iridescent cellulose nanocrystal films. *Adv Mater* 29:256–262. <https://doi.org/10.1002/adma.201603560>
- Filson PB, Dawson-Andoh BE (2009) Sono-chemical preparation of cellulose nanocrystals from lignocellulose derived materials. *Bioresource Technol* 100:2259–2264. <https://doi.org/10.1016/j.biortech.2008.09.062>
- Gan L, Liao J, Lin N, Hu C, Wang H, Huang J (2017) Focus on gradientwise control of the surface acetylation of cellulose nanocrystals to optimize mechanical reinforcement for hydrophobic polyester-based nanocomposites. *ACS Omega* 2:4725–4736. <https://doi.org/10.1021/acsomega.7b00532>
- Giese M, Blusch LK, Khan MK, MacLachlan MJ (2015) Functional materials from cellulose-derived liquid-crystal templates. *Angew Chem* 54:2888–2910. <https://doi.org/10.1002/anie.201407141>
- Hamad WY, Hu TQ (2010) Structure–process–yield interrelations in nanocrystalline cellulose extraction. *Can J Chem Eng* 88:392–402. <https://doi.org/10.1002/cjce.20298>
- Kang X, Kuga S, Wang C, Zhao Y, Wu M, Huang Y (2018) Green preparation of cellulose nanocrystal and its application. *ACS Sustain Chem Eng* 6:2954–2960. <https://doi.org/10.1021/acssuschemeng.7b02363>
- Kontturi E et al (2016) Degradation and crystallization of cellulose in hydrogen chloride vapor for high-yield isolation of cellulose nanocrystals. *Angew Chem Int Ed* 55:14455–14458. <https://doi.org/10.1002/anie.201606626>
- Lagerwall JPF, Schütz C, Salajkova M, Park JH (2014) Cellulose nanocrystal-based materials: from liquid crystal self-assembly and glass formation to multifunctional thin films NPG. *Asia Mater* 6:e80. <https://doi.org/10.1038/am.2013.69>
- Li Y, Liu Y, Chen W, Wang Q, Liu Y, Li J, Yu H (2016) Facile extraction of cellulose nanocrystals from wood using ethanol and peroxide solvothermal pretreatment followed by ultrasonic nanofibrillation. *Green Chem* 18:1010–1018. <https://doi.org/10.1039/c5gc02576a>
- Li D, Henschen J, Ek M (2017) Esterification and hydrolysis of cellulose using oxalic acid dihydrate in a solvent-free reaction suitable for preparation of surface-functionalised cellulose nanocrystals with high yield. *Green Chem* 10:352–355. <https://doi.org/10.1039/c7gc02489d>
- Liu YJ, Cao WT, Ma MG, Wan P (2017) Ultrasensitive wearable soft strain sensors of conductive, self-healing, and elastic hydrogels with synergistic “soft and hard” hybrid networks. *ACS Appl Mater Interfaces* 9:25559–25570. <https://doi.org/10.1021/acsami.7b07639>
- Lu Q, Cai Z, Lin F, Tang L, Wang S, Huang B (2016) Extraction of cellulose nanocrystals with a high yield of 88% by simultaneous mechanochemical activation and phosphotungstic acid hydrolysis. *ACS Sustain Chem Eng*

- 4:2165–2172. <https://doi.org/10.1021/acssuschemeng.5b01620>
- Mishra SP, Thirree J, Manent AS, Chabot B, Daneault C (2011) Ultrasound-catalyzed TEMPO-mediated oxidation of native cellulose for the production of nanocellulose: effect of process variables. *BioResources* 6:121–143
- Park S, Baker JO, Himmel ME, Parilla PA, Johnson DK (2010) Cellulose crystallinity index: measurement techniques and their impact on interpreting cellulase performance. *Biotechnol Biofuels* 3:210–219. <https://doi.org/10.1186/1754-6834-3-10>
- Reid MS, Kedzior SA, Villalobos M, Cranston ED (2017) Effect of ionic strength and surface charge density on the kinetics of cellulose nanocrystal thin film swelling. *Langmuir* 33:7403–7411. <https://doi.org/10.1021/acs.langmuir.7b01740>
- Schutyser W et al (2018) Revisiting alkaline aerobic lignin oxidation. *Green Chem* 20:3828–3844. <https://doi.org/10.1039/c8gc00502h>
- Shopsowitz KE, Qi H, Hamad WY, MacLachlan MJ (2010) Free-standing mesoporous silica films with tunable chiral nematic structures. *Nature* 468:422–425. <https://doi.org/10.1038/nature09540>
- Shopsowitz KE, Hamad WY, MacLachlan MJ (2011) Chiral nematic mesoporous carbon derived from nanocrystalline cellulose. *Angew Chem* 50:10991–10995. <https://doi.org/10.1002/anie.201105479>
- Shopsowitz KE, Kelly JA, Hamad WY, MacLachlan MJ (2014) Biopolymer templated glass with a twist: controlling the chirality, porosity, and photonic properties of silica with cellulose nanocrystals. *Adv Funct Mater* 24:327–338. <https://doi.org/10.1002/adfm.201301737>
- Sluiter A, Hames B, Ruiz R, C. Scarlata, Sluiter J, Templeton D, Crocker D (2012) Determination of structural carbohydrates and lignin in biomass. National Renewable Energy Laboratory NREL/TP-510-42618
- Tang L, Huang B, Lu Q, Wang S, Ou W, Lin W, Chen X (2013) Ultrasonication-assisted manufacture of cellulose nanocrystals esterified with acetic acid. *Bioresour Technol* 127C:100–105. <https://doi.org/10.1016/j.biortech.2012.09.133>
- Tang H, Butchosa N, Zhou Q (2015) A transparent, hazy, and strong macroscopic ribbon of oriented cellulose nanofibrils bearing poly(ethylene glycol). *Adv Mater* 27:2070–2076. <https://doi.org/10.1002/adma.201404565>
- Teramura H et al (2016) Organosolv pretreatment of sorghum bagasse using a low concentration of hydrophobic solvents such as 1-butanol or 1-pentanol. *Biotechnol Biofuels* 9:27–37. <https://doi.org/10.1186/s13068-016-0427-z>
- Wang PX, Hamad WY, MacLachlan MJ (2016) Structure and transformation of tactoids in cellulose nanocrystal suspensions. *Nat Commun* 7:11515. <https://doi.org/10.1038/ncomms11515>
- Yao K, Meng Q, Bulone V, Zhou Q (2017) Flexible and responsive chiral nematic cellulose nanocrystal/poly(ethylene glycol) composite films with uniform and tunable structural color. *Adv Mater* 29:1701323–1701330. <https://doi.org/10.1002/adma.201701323>
- Yarbrough JM et al (2017) Multifunctional cellulolytic enzymes outperform processive fungal cellulases for coproduction of nanocellulose and biofuels. *ACS Nano* 11:3101–3109. <https://doi.org/10.1021/acsnano.7b00086>
- Zander NE, Dong H, Steele J, Grant JT (2014) Metal cation cross-linked nanocellulose hydrogels as tissue engineering substrates. *ACS Appl Mater Interfaces* 6:18502–18510. <https://doi.org/10.1021/am506007z>
- Zhang R, Liu Y (2018) High energy oxidation and organosolv solubilization for high yield isolation of cellulose nanocrystals (CNC) from Eucalyptus hardwood. *Sci Rep* 8:16505. <https://doi.org/10.1038/s41598-018-34667-2>
- Zhou H, Zhang R, Zhan W, Wang L, Guo L, Liu Y (2016) High biomass loadings of 40 wt% for efficient fractionation in biorefineries with an aqueous solvent system without adding adsorbent catalyst. *Green Chem* 18:6108–6114. <https://doi.org/10.1039/c6gc02225a>
- Zhou Y, Saito T, Bergstrom L, Isogai A (2018) Acid-free preparation of cellulose nanocrystals by TEMPO oxidation and subsequent cavitation. *Biomacromol* 19:633–639. <https://doi.org/10.1021/acs.biomac.7b01730>

Publisher's Note Springer Nature remains neutral with regard to jurisdictional claims in published maps and institutional affiliations.